MNRAS **435,** 2822–2834 (2013)
Advance Access publication 2013 September 21
doi:10.1093/mnras/stt1434

On the nature of the hard X-ray sources SWIFT J1907.3−2050, IGR J12123−5802 and IGR J19552+0044

F. Bernardini,[1,2]★ D. de Martino,[2] K. Mukai,[3,4] M. Falanga,[5] I. Andruchow,[6] J.-M. Bonnet-Bidaud,[7] N. Masetti,[8] D. H. Gonzalez Buitrago,[9] M. Mouchet[10,11] and G. Tovmassian[9]

[1]*Wayne State University, 666 W. Hancock Street, Detroit, MI 48201, USA*
[2]*INAF − Osservatorio Astronomico di Capodimonte, Salita Moiairiello 16, I-80131 Napoli, Italy*
[3]*CRESST and X-Ray Astrophysics Laboratory, NASA Goddard Space Flight Center, Greenbelt, MD 20771, USA*
[4]*Department of Physics, University of Maryland, Baltimore County, 1000 Hilltop Circle, Baltimore, MD 21250, USA*
[5]*International Space Science Institute (ISSI), Hallerstrasse 6, CH-3012 Bern, Switzerland*
[6]*Facultad de Ciencias Astronomicas y Geofisicas, UNLP, and Instituto de Astrofisica La Plata, CONICET/UNLP, Argentina*
[7]*CEA Saclay, DSM/Irfu/Service d'Astrophysique, F-91191, Gif-sur-Yvette, France*
[8]*INAF − Istituto Astrofisica Spaziale, Via Gobetti 101, I-40129, Bologna, Italy*
[9]*Instituto de Astronomia, Universidad Nacional Autonoma de Mexico, Apdo. Postal 877, Ensenada, Baja California 22800, Mexico*
[10]*Laboratoire APC, Université Denis Diderot, 10 rue Alice Domon et Léonie Duquet, F-75005 Paris, France*
[11]*LUTH, Observatoire de Paris, Section de Meudon, 5 place Jules Janssen, F-92195 Meudon, France*

Accepted 2013 July 30. Received 2013 July 25; in original form 2013 June 19

ABSTRACT

The *INTEGRAL* and *Swift* hard X-ray surveys have identified a large number of new sources, among which many are proposed as Cataclysmic Variables (CVs). Here, we present the first detailed study of three X-ray-selected CVs, Swift J1907.3−2050, IGR J12123−5802 and IGR J19552+0044 based on *XMM–Newton*, *Suzaku*, *Swift* observations and ground-based optical and archival (near-IR) nIR/IR data. Swift J1907.3−2050 is highly variable from hours to months–years at all wavelengths. No coherent X-ray pulses are detected but rather transient features. The X-ray spectrum reveals a multitemperature optically thin plasma absorbed by complex neutral material and a soft blackbody component arising from a small area. These characteristics are remarkably similar to those observed in magnetic CVs. A supra-solar abundance of nitrogen could arise from nuclear processed material from the donor star. Swift J1907.3−2050 could be a peculiar magnetic CV with the second longest (20.82 h) binary period. IGR J12123−5802 is variable in the X-rays on a time-scale of $\gtrsim$7.6 h. No coherent pulsations are detected, but its spectral characteristics suggest that it could be a magnetic CV of the Intermediate Polar (IP) type. IGR J19552+0044 shows two X-ray periods, ∼1.38 h and ∼1.69 h and an X-ray spectrum characterized by a multitemperature plasma with little absorption. We derive a low accretion rate, consistent with a CV below the orbital period gap. Its peculiar nIR/IR spectrum suggests a contribution from cyclotron emission. It could either be a pre-polar or an IP with the lowest degree of asynchronism.

Key words: X-rays: individual: Swift J1907.3−2050 (also known as: V1082 Sgr) – X-rays: individual: Swift J1212.3−5806 (also known as: IGR J12123−5802 and 1RXS J121222.7−580118) – X-rays: individual: IGR J19552+0044 – X-rays: individual: WISE J195512.47+004536.6.

1 INTRODUCTION

Cataclysmic Variable stars (CVs) are binary system in which a white dwarf (WD) accretes matter from a late-type main-sequence or sub-giant star. A large fraction, ∼20–25 per cent (see e.g. Wickramasinghe & Ferrario 2000; Pretorius, Knigge & Schwope 2013, and reference therein) of whole CV class, harbours-magnetized WDs with $B \gtrsim 10^5$ G up to 2.3 × 10^8 G. The high magnetic systems, the Polars, show intense and variable polarized emission in the optical and near-IR (nIR) ranges, while those showing weakly or unpolarized optical/nIR emission, the Intermediate

★E-mail: bernardini@wayne.edu

Polars (IPs), are believed to possess weaker $B \leq 10^6$ G. They are both characterized by variable X-ray emission at the rotational period of the accreting WD that is $P_{\rm rot}/P_{\rm orb} \simeq 1$ in the Polars (synchronous systems) and $P_{\rm rot}/P_{\rm orb} < 1$ in the IPs (asynchronous systems). The latter group is generally found above the 2–3 h orbital period gap, whilst the Polars populate the orbital period distribution at short values, mainly below the gap (see Warner 1995).

The hard X-ray surveys carried out above 20 keV by the *INTEGRAL* and *Swift* satellites have detected more than a thousand of sources, a non-negligible fraction (∼6 per cent) of them are galactic X-ray binaries containing WDs (Barlow et al. 2006; Bird et al. 2010; Cusumano et al. 2010; Baumgartner et al. 2013). The confirmed CVs detected in these surveys are mainly maFVgnetic of the IP type (∼80 per cent of the whole sample). A few Polars and a handful of non-magnetic systems that include dwarf novae, old novae and nova-like CVs, the latter still disputed to be magnetic, are also present. Finally, a few symbiotic stars have been also detected (see e.g. Luna et al. 2012). The current roster of these hard X-ray accreting WDs totals to 67, about half of them have been first proposed as CV candidates through optical spectroscopic follow-ups (e.g. Masetti et al. 2006, 2008, 2010, 2012) and many are suspected to harbour a magnetic WD. However, only X-ray follow-ups, mainly conducted with *XMM–Newton*, allowed us to unambiguously confirm (de Martino et al. 2008; Anzolin et al. 2009; Scaringi et al. 2011; Bernardini et al. 2012; Masetti, Nucita & Parisi 2012) or reject (de Martino et al. 2010, 2013) a CV identification, thanks to the detection (or non-detection) of an X-ray signal at the WD spin period and to the characterization of the X-ray spectral properties. However, so far, there are several tens of sources to be still identified.

The role of CVs in the galactic population of X-ray sources has been quite discussed recently. In particular, magnetic CVs, are claimed to represent a large population (thousands of sources), and to be dominant contributors to the Galactic Ridge X-ray Emission (GRXE) and bulge emission (Revnivtsev et al. 2011; Hong et al. 2012; Hong 2012) at low luminosities (i.e. below 10^{33} erg s^{-1}). However, the bulk of the CV population that is dominated by non-magnetic short orbital period systems, can account for the very low end ($<10^{30}$ erg s^{-1}) of the GRXE luminosity function (Reis et al. 2013), while magnetic CVs are believed to contribute most at $\gtrsim 10^{30}$ erg s^{-1} (Hong 2012). The contribution from X-ray active stars at very low luminosities is still debated. The ratio of WD binaries and of coronally active stars is believed to be ∼2:1 (Morihana et al. 2013; Nebot Gómez-Morán et al. 2013).

In magnetic CVs, the accretion flow is magnetically channelled on to the WD polar regions. A strong shock is formed, below which matter cools via thermal bremsstrahlung and cyclotron radiation, the relative proportion primarily depending on the WD magnetic field strength (Woelk & Beuermann 1996; Fischer & Beuermann 2001). Hence, low-field magnetic CVs, like the IPs, have bremsstrahlung dominated shocks, while the Polars mainly cool via cyclotron radiation. Thus, IPs were initially known to be bright harder X-ray sources than the Polars. However, before the deep surveys by *INTEGRAL* and *Swift* they only constituted a minor fraction of the magnetic CV sub-class. This view has now changed with the identification of new magnetic systems of this type, suggesting that our knowledge of the magnetic CV population, and hence evolution, is still poor.

The identification of new hard X-ray CVs, can allow us to put constraints on the true contribution of these binaries to the whole CV population as well as to identify new unexplored properties. Most of the *INTEGRAL* and *Swift* hard X-ray CVs are found at long orbital periods ($\gtrsim$5 h), with a few exceptions, and possess rapidly rotating WDs with spin-to-orbit period ratios ≤0.12 (Bernardini et al. 2012). This view could be confirmed or changed by the characterization of a larger sample, so that the role of system parameters, such as the WD magnetic field, the WD mass and the mass accretion rate, can be finally unveiled. In this work, we present the first X-ray observations of a sample of three magnetic CV candidates, all hard X-ray sources: Swift J1907.3−2050, IGR J12123−5802 and IGR J19552+0044 (henceforth Swift J1907, IGR J1212 and IGR J1955). We complement the X-ray study with simultaneous UV and optical photometry acquired with the *XMM–Newton* satellite and with ground-based optical and archival nIR/IR data. Swift J1907 is also known as V1082 Sgr, a long (20.82 h) orbital period CV suggested as a possible magnetic system by Thorstensen, Peters & Skinner (2010) because of the hard X-ray detection. IGR J1212 and IGR J1955 were identified by Masetti et al. (2010) from optical spectroscopic follow-ups as CVs and also suspected to be magnetic because of characteristics of their emission lines. No further information on these sources are available to date. Our study reveals unusual temporal and spectral properties that make these sources interesting cases for further follow-ups at other wavelengths.

2 OBSERVATIONS AND DATA ANALYSIS

2.1 *XMM–Newton* observations

The three sources were all observed in 2012 by the *XMM–Newton* observatory, (den Herder et al. 2001; Mason et al. 2001; Turner et al. 2001), using the EPIC cameras as main instruments. The details of the *XMM–Newton* observations, together with that of *Swift* and *Suzaku* are reported in Table 1. All data were processed and scientific products were extracted with SAS version 12.0.1 using the latest calibration files (CCF) available in 2012 September (EPIC and OM) and 2013 May (RGS).

2.1.1 The EPIC and RGS data

All observations were performed with the EPIC PN and MOS cameras set in prime full window imaging mode with the thin filter. Standard data screening criteria were applied for all instruments.

For EPIC data, we extracted source photons from circular regions of radius 35 arcsec centred on source position determined by Gaussian fitting on one-dimension photon distribution. The background photons were extracted from a circular region of same size within the same CCD. To avoid contamination from solar flares in the spectral analysis, we conservatively produced spectra using only those parts of the observations free from high background epochs. For the timing analysis, we instead used the whole data sets except Swift J1907 for which contamination from solar flares is particularly strong at the end of the EPIC exposure. Background-subtracted light curves were produced in the ranges: 0.3–15 keV (with a bin time of 15 s), 0.3–1 keV, 1–3 keV, 3–5 keV and 5–15 keV (with a bin time of 75 s). For each source, event arrival times were corrected to Solar system barycenter. The EPIC spectra were rebinned before fitting, to have at least 30 counts per bin. We report the spectral analysis results obtained with the PN data only (consistency with the results of MOS cameras was always verified). Phase–resolved spectra were also extracted at the pulse maximum and minimum.

The RGS spectra were extracted using the whole exposures except Swift J1907 for which only the first 21 ks of data were retained. Due to low count rates, we only inspected the first-order spectra for all three sources; however, for IGR J1212, even the first-order spectra were too noisy to allow a spectral study. For Swift J1907 and

Table 1. Summary of main observations parameters for all instruments.

Source	Telescope	OBSID	Instrument	Date (yyyy-mm-dd)	UT_{start} (hh:mm)	T_{expo} (ks)[a]	Net Count Rate cts s^{-1}
Swift J1907.3−2050	*XMM–Newton*	0671 850 301	EPIC-pn	2012-03-19	11:32	38.0/13.6[b]	4.54 ± 0.02
			EPIC-MOS1	2012-03-19	11:10	27.2	1.10 ± 0.07
			EPIC-MOS2	2012-03-19	11:10	27.2	1.16 ± 0.07
			RGS1	2012-03-19	11:10	36.5/20.9[c]	0.082 ± 0.003
			RGS2	2012-03-19	11:10	36.5/20.9[c]	0.093 ± 0.003
			OM-B	2012-03-19	11:20	18.8	79.82 ± 0.02
			OM-UVM2	2012-03-19	17:00	18.8	6.52 ± 0.04
	Suzaku	406 042 010	XIS0	2012-03-23	05:32	39.5	0.692 ± 0.004
	Suzaku		XIS1	2012-03-23	05:32	39.5	0.796 ± 0.005
	Suzaku		XIS3	2012-03-23	05:32	39.5	0.750 ± 0.005
	Swift	[d]	BAT			5800	$3.5 \pm 0.4 \times 10^{-4}$
		00 037 329 001	XRT	2008-04-10	13:38	3.5	0.25 ± 0.01
		00 037 329 002	XRT	2008-06-04	15:57	0.4	0.13 ± 0.02
		00 037 329 003	XRT	2008-06-12	13:23	1.0	0.23 ± 0.02
		00 037 329 004	XRT	2008-06-12	15:01	0.3	0.23 ± 0.02
		00 037 329 005	XRT	2008-06-13	08:23	0.4	0.36 ± 0.03
		00 037 329 006	XRT	2008-06-13	10:20	0.1	0.36 ± 0.01
		00 037 329 008	XRT	2008-06-26	00:31	1.4	0.10 ± 0.01
		00 031 252 001	XRT	2008-08-19	06:54	1.3	0.05 ± 0.01
		00 031 252 002	XRT	2008-08-20	11:41	10.1	0.030 ± 0.003
		00 031 252 003	XRT	2008-08-28	07:36	1.9	0.05 ± 0.01
		00 037 329 009	XRT	2008-11-14	12:01	5.2	0.017 ± 0.002
		00 031 252 004	XRT	2012-06-19	12:32	3.4	0.002 ± 0.001
		00 031 252 005	XRT	2012-06-20	01:33	6.4	0.002 ± 0.001
IGR J12123−5802	*XMM–Newton*	0671 850 601	EPIC-pn	2012-01-07	15:48	37.4/12[b]	0.754 ± 0.008
			EPIC-MOS1	2012-01-07	15:26	39.6	0.255 ± 0.003
			EPIC-MOS2	2012-01-07	15:26	39.6	0.259 ± 0.003
			RGS1	2012-01-07	15:25	40.1	0.010 ± 0.002
			RGS2	2012-01-07	15:25	40.1	0.012 ± 0.002
			OM - V	2012-01-07	15:35	15.8	2.33 ± 0.03
			OM - UVM2	2012-01-07	21:38	15.8	0.27 ± 0.2
	Swift	[d]	BAT			7500	$1.8 \pm 0.3 \times 10^{-4}$
IGR J19552+0044	*XMM–Newton*	0671 850 201	EPIC-pn	2012-04-29	06:04	38/19[b]	2.88 ± 0.02
			EPIC-MOS1	2012-04-29	05:41	39	0.647 ± 0.005
			EPIC-MOS2	2012-04-29	05:41	39	0.630 ± 0.005
			RGS1	2012-04-29	05:41	36.8	0.054 ± 0.002
			RGS2	2012-04-29	05:41	36.8	0.071 ± 0.002
			OM-B	2012-04-29	05:50	15.8	4.87 ± 0.02
			OM-UVM2	2012-04-29	10:40	15.8	0.65 ± 0.02

[a]Net exposure times.
[b]We report both the total exposure time and that after removing solar flares.
[c]We report both the total exposure and that during the low background interval.
[d]All available pointings are summed together.

IGR J1955, we grouped channels so each had at least 16 source counts, after ignoring extreme ends of the RGS energy ranges and the ranges corresponding to the inoperative CCD chips. Given the low statistical quality and the limited energy range of the RGS data, we used them mainly to confirm and refine the best-fitting model derived using the EPIC data.

All spectra were analysed using the version of xspec (12.7.1n).

2.1.2 The optical monitor photometry

The optical monitor (OM) instrument was operated in fast window mode during all observations of the three sources. The OM data of Swift J1907 and of IGR J1955 were collected in two photometric bands using first the *B* filter, centred at 4500 Å and then the *UVM2* filter, centred at 2310 Å. For IGR J1212 we instead used the *V* filter, centred at 5430 Å, due to brightness limits of a close-by star in the OM field of view. In this way, we obtained two time series sets for each source 18.8 ks (Swift J1907), 16.6 ks (IGR J1212) and 15.8 ks (IGR J1955) long. The OM light curves were obtained from the SAS processing pipeline with a binning time of 10 s or 20 s. Corrections to the solar barycenter were also applied to the OM light curves.

2.2 The *Suzaku* observation

Swift J1907 was also observed with *Suzaku* (Mitsuda et al. 2007) in 2012 March, a few days after the *XMM–Newton* observation. Here, we include the timing analysis of the data taken with the X-ray imaging spectrometer (XIS; Koyama et al. 2007). We have taken the data as processed using pipeline version 2.7.16.32, and extracted the source light curves from a circular region of 3.50 arcmin radius centred on the source image. Background light curves were extracted from an annular region with outer and inner radii of 6.25

and 4.50 arcmin, respectively, and subtracted from the source region curves after scaling by the ratio of the extraction regions (0.65). Light curves from all three active XIS units have been combined in our analysis.

2.3 The *Swift* observations

The *Swift* Burst Alert Telescope, BAT (Barthelmy 2000), is a wide-field (∼1 sr) coded aperture mask instrument sensitive in the 14–195 keV range. Thanks to the large field of view, BAT has built up a sensitive all-sky map of the hard X-ray sky. We have taken the eight-channel spectra from the first 58 months of the mission.[1] We collected BAT data of Swift J1907 and IGR J1212, while no data of IGR J1955 are available. IGR J1955 is also too faint to use the *INTEGRAL* IBIS/ISGRI spectral data, the source being at an average rate of 0.06 ± 0.02 cts s^{-1} in the 20–40 keV.[2] Therefore, we have extended the spectral analysis above 10 keV for Swift J1907 and IGR J1212 only.

The *Swift* X-ray Telescope (XRT, Gehrels et al. 2004) is an imaging CCD spectrometer sensitive in the 0.3–10 keV range. *Swift* performed 13 short (few ks) pointings of Swift J1907, 11 in 2008 and 2 in 2012. A total of about 35 ks of exposure time was collected on this source. We used the *Swift*/XRT data products generator at the University of Leicester (Evans et al. 2009) to build the background-subtracted light curve and the average spectrum in photon counting (PC) mode of Swift J1907.

3 RESULTS

3.1 Swift J1907.3−2050

3.1.1 X-ray timing analysis

The PN 0.3–15 keV light curve is highly variable (Fig. 1) with count rate changing by more than 60 per cent. A long-term trend could also be present, with a time-scale larger than 8 h, but the exposure (only 10.6 h) is not long enough to characterize this variability. The stronger variations are detected on shorter time-scale (∼2 h) after the first 10 ks since the start of the observation. The 0.3–15 keV power spectrum of the total observation (Fig. 1) shows an asymmetric peak at ∼0.000 139 Hz with an excess at lower frequencies. The first harmonic is also present and there is also indication of power at a lower frequency ($\sim 4 \times 10^{-5}$ Hz). The main peak would correspond to a period of 7200 ± 500 s (2.00 ± 0.14 h), see also Table 2. All uncertainties are hereafter at 1σ confidence level if not otherwise specified. However, a closer inspection of the light curve in three time intervals: 0–10 ks, 10–25 ks and 25–38 ks does not reveal pulses above 3σ significance, except in the 10–25 ks interval, where the Pulse Fraction (PF)[3] is 32.7 ± 0.6 per cent. Therefore, the ∼2 h X-ray signal does not appear to be coherent. The extracted light curves in the four energy bands 0.3–1, 1–3, 3–5 and 5–15 keV in the 10–25 ks time interval reveal that this transient variability is energy dependent, with PF decreasing from 38 ± 1 per cent in the 0.3–1 keV band to 28 ± 1 per cent in the hard 5–15 keV band.

[1] http://swift.gsfc.nasa.gov/docs/swift/results/bs58mon/

[2] http://www.isdc.unige.ch/heavens/

[3] The pulse fraction is here defined as $\mathrm{PF} = (A_{\max} - A_{\min})/(A_{\max} + A_{\min})$, where $A_{\max}$ and $A_{\min}$ are, respectively, the maximum and minimum value of a sinusoidal function.

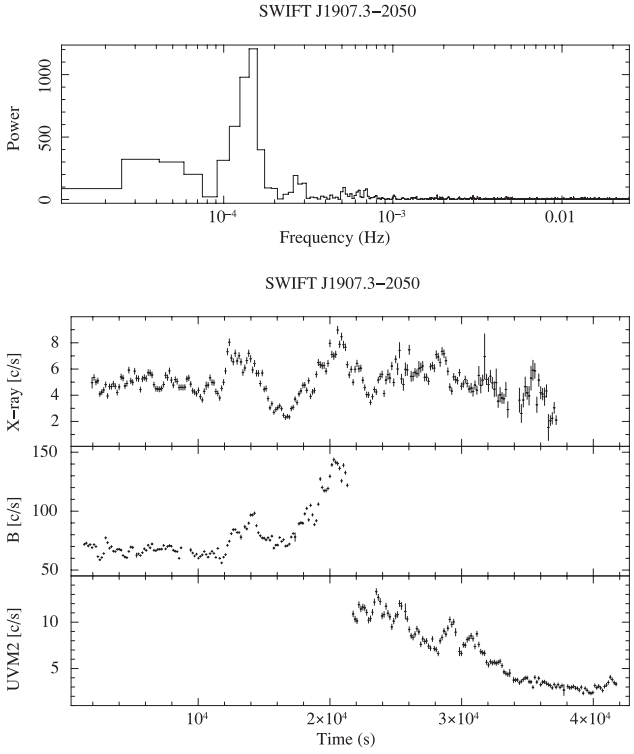

Figure 1. Upper Panel: Swift J1907 PN 0.3–15 keV power spectrum. Lower Panels: Swift J1907 background-subtracted light curve in three energy bands: PN 0.3–15 keV (top), *B* (centre), *UVM2* (bottom). The binning time is 150 s in all bands.

Table 2. Summary of the main timing results for the three sources. From left to right: $P^X_{1,2}$ (X-ray periods); $P^X_{\rm lt}$ (X-ray long-term trend).

Source	$P^X_{1,2}$ [a] (s)	$P^X_{\rm lt}$ [b] (h)
Swift J1907	7200 ± 500 [c]	>8.4
IGR J1212	–	7.6 ± 0.1
IGR J1955	6100 ± 120, 4960 ± 80	11.4 ± 0.2

[a] 1σ cl.
[b] 3σ cl. $P^X_{\rm lt}$ must be interpreted as an indication of long term variability.
[c] This signal is not coherent.

The *Suzaku* X-ray light curve, spanning over ∼28.6 ks, includes a prominent brightening (hereafter 'flare') starting roughly halfway through the observation and lasting for three spacecraft orbits (5–6 h). We have extracted the hard (>2 keV) and soft (<2 keV) light curves separately, but the hardness ratio (HR) does not show a significant change during the flare (Fig. 2). A Fourier analysis of the entire data set (without energy cut) shows substantial power at low frequencies, including a peak near 2 h, but no significant peaks at higher frequencies (Fig. 3). We analysed the flare and non-flare data separately and found that the 2 h peak is not persistent through the observation; it is definitely absent in the non-flare data. While some power near this frequency may well be present in the flare data, no definite conclusion can be made due to the relatively short duration of the flare and the *Suzaku* orbital gaps.

We also inspected the *Swift*/XRT PC data of Swift J1907 to search for similar variabilities. The source count rate changes along the total baseline (1533 d) from a maximum of ∼0.5 cts s^{-1} to a

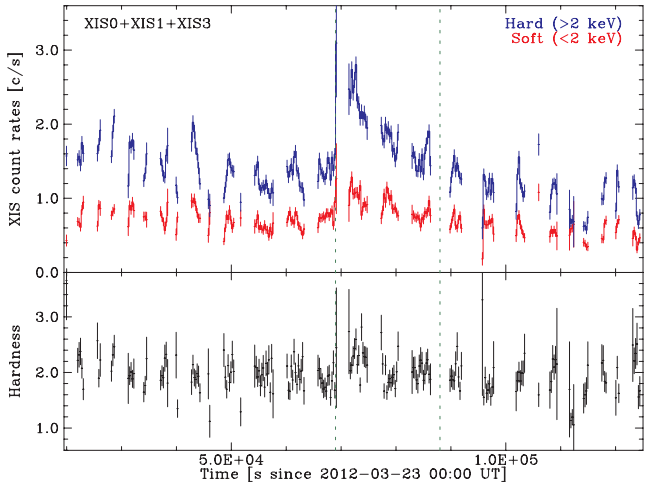

Figure 2. Swift J1907: (Upper panel) *Suzaku*/XIS light curves of Swift J1907, in two energy bands. (Lower panel) The hardness ratio (HR) as a function of time. The vertical dashed lines define the flare interval used in Fourier analysis.

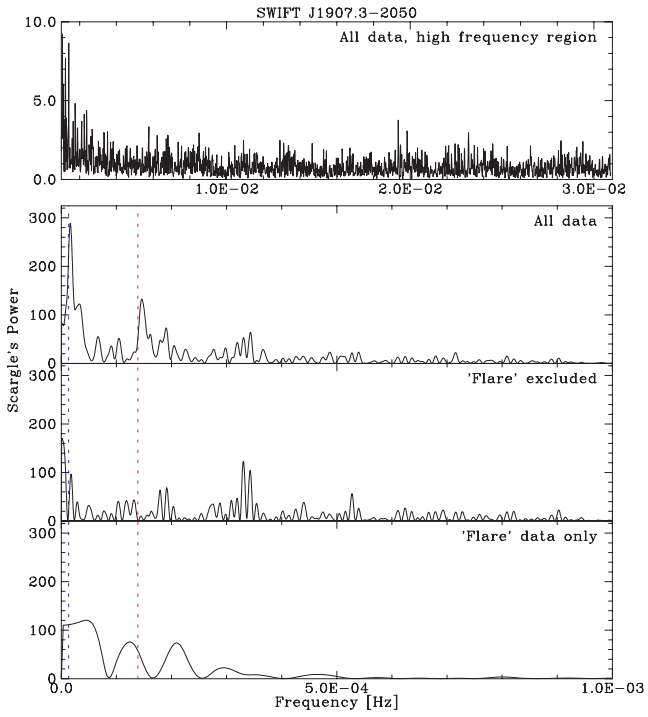

Figure 3. Swift J1907: power spectra of *Suzaku*/XIS data using Scargle's definition (Scargle 1982). The top panel shows the high-frequency region of the power spectrum for all data. The bottom panels show the low-frequency region, for the entire data, the non-flare data and the flare data only, from top to bottom. The vertical dashed lines correspond to the 2 h variability detected in the *XMM–Newton* data.

minimum of 0.002 cts s^{-1} (see Fig. 4). In particular, we note that the two 2012 *Swift*/XRT observations carried out in June, three months after the *XMM–Newton* and *Suzaku* pointings, show the lowest count rate (0.002 cts s^{-1}). Furthermore, hints for short term periodic-like variability, of the order of two hours, consistent with that measured in the *XMM–Newton* data, is found in a selected light-curve sub-interval, where the *Swift* coverage was more dense (between $d \sim 132$ and $d \sim 132.4$ reference time BJD = 245 4567.0708). However, due to the satellite gaps we cannot further constrain this variability.

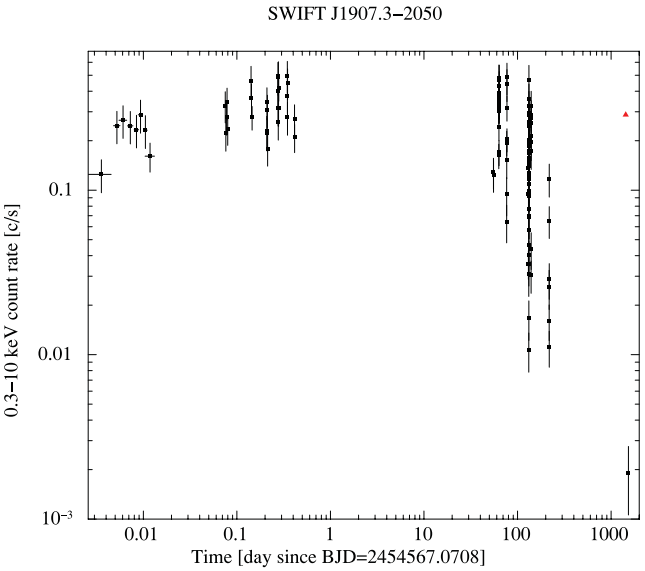

Figure 4. *Swift*/XRT light curve of Swift J1907. Due to the extremely sparse coverage, for plotting purposes, data are shown on a logarithmic scale. The black squares represent *Swift* data. The red triangle represent the estimated 0.5–10 keV *Swift* count rate for the *XMM–Newton* and the *Suzaku* 2012 pointings. We estimated it with *webpimms* using a power law multiplied by local and galactic absorption as a spectral model.

3.1.2 *The UV and optical light curves*

Swift J1907 is at 13.14 ± 0.09 mag and at 14.70 ± 0.04 mag in the *UVM2* and the *B* band, respectively, corresponding to fluxes of 1.43×10^{-14} erg cm^{-2} s^{-1} $Å^{-1}$ and to 1.03×10^{-14} erg cm^{-2} s^{-1} $Å^{-1}$.

The UV and optical light curves are also highly variable (see Fig. 1) with a strong rise in the *B* band count rate after 12 ks, coincident in time with the X-ray flux increase. Both the X-ray and *B* light curves display a first maximum at ∼13 ks and a second at ∼20 ks. In the subsequent UV exposure, the count rate decreases by a factor of 2.2 at the end of the pointing.

We also divided the *B*-band light curve in two intervals, I: 0–10 ks and II: 10–22 ks, while we selected for the *UVM2* light curve only the 22–38 ks interval (interval III). Then, we cross-correlated the X-ray (used as reference) with the *B*- and *UWM2*-band light curves in the three intervals. The cross-correlation function (CCF) in interval II is broad and asymmetric towards negative lags, with degree of correlation 0.6. For CCFs with complex shapes or asymmetries the centroid is best evaluated using time lags in excess of 0.8 the peak value (e.g. Peterson et al. 1998; Shang 2002). We then find $t_{\rm cent} \simeq -310$ s. The significance of the correlation is 15σ. Instead, no correlation is found in interval I, while for interval II a weak degree of correlation is found (0.2). Hence, we can then conclude that the optical light leads the X-rays in the II interval only and that the transient signal is also present at optical wavelengths.

3.1.3 *X-ray Spectral analysis*

The combined *XMM–Newton* EPIC and *Swift* BAT (0.3–100 keV) average spectrum was first fitted by a single optically thin component (MEKAL) multiplied by a complex absorption that includes a total absorber (WABS) and a partial covering absorber (PCFABS). The latter is justified by the energy dependence of the transient

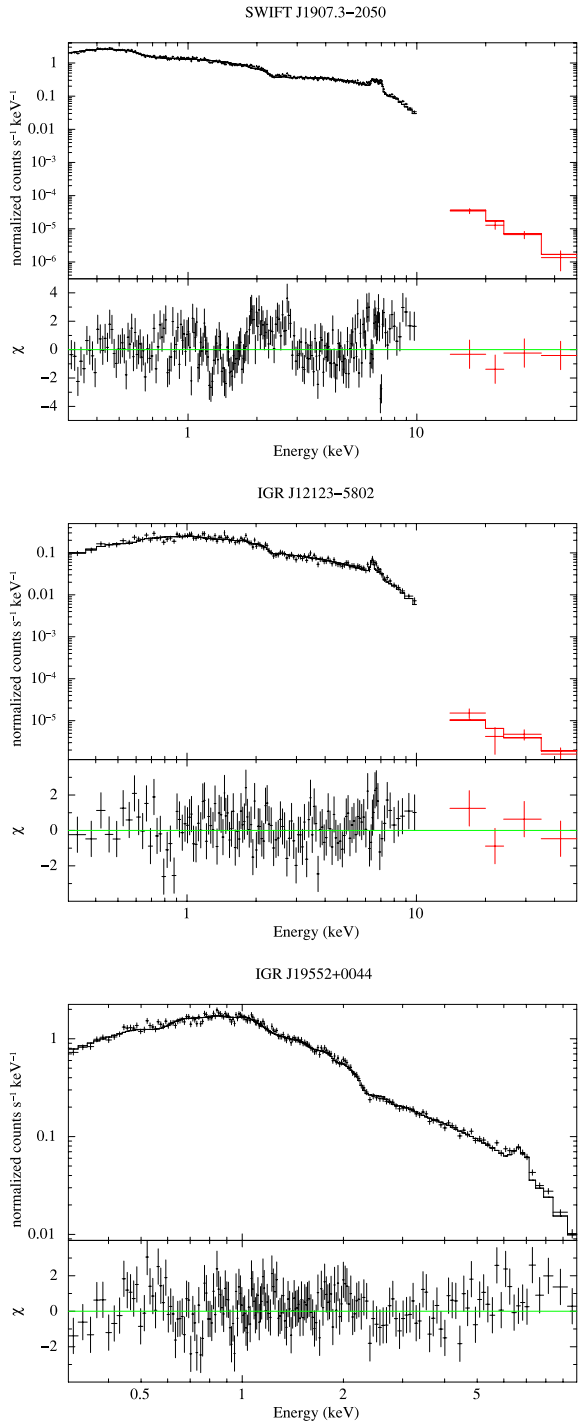

Figure 5. Upper panels: Swift J1907 broad-band 0.3–100 keV count spectrum. Data are rebinned for plotting purposes. XMM data are in black while *Swift*/BAT data are in red. Residuals are shown in the bottom panel. Center panels: the same as above, but for IGR J1212. Here the CEMEKL model is shown. Lower panels: the same as above, but for IGR J1955, in the range 0.3–10 keV only (no BAT data are available). Here the CEMEKL model is shown.

signal. This gives a poor fit ($\chi^2_\nu = 2.05$ for 1000 d.o.f.). Substantial improvements are found including additional components and verifying their statistical significance (greater than 3σ) with an *F*-test. We then obtain the best-fitting model (see Fig. 5) consisting of two MEKAL components, a cold (c) at 0.12 ± 0.02 keV and a hot (h) at

Table 3. Swift J1907: spectral parameters of the best-fitting model. Uncertainties are 1 sigma confidence level.

	Swift J1907 BB+2 MEKAL	
$N_{\rm H_W}$	10^{22} cm^{-2}	0.103 ± 0.006
$N_{\rm H_{Pc}}$	10^{22} cm^{-2}	9.6 ± 0.5
cvf	per cent	67 ± 1
$kT_{\rm BB}$	eV	61 ± 5
$kT_{\rm c}$	keV	0.12 ± 0.02
$kT_{\rm h}$	keV	13.2 ± 0.6
$R_{\rm BB}$	km	40^{+20}_{-10}
norm$_{\rm c}$	10^{-3}	$5^{+0.3}_{-0.9}$
norm$_{\rm h}$	10^{-3}	20.1 ± 0.5
A$_{\rm Z}$		0.70 ± 0.05
EW[a]	keV	0.15 ± 0.01
$F_{0.3-10}$	10^{-11}	2.45 ± 0.05
F_{15-100}	10^{-11}	1.3 ± 0.1
$F^{BB\ b}_{\rm bol}$	10^{-11}	$\sim$2.9
$F^{c+h\ c}_{\rm bol}$	10^{-11}	$\sim$12
χ^2_ν (d.o.f.)		1.15 (995)

[a]Gaussian energy fixed at 6.4 keV.
[b]Unabsorbed bolometric flux of the blackbody component.
[c]Unabsorbed bolometric flux of the two optically thin components.

13.2 ± 0.6 keV, plus an optically thick (BB) component at 61 ± 5 eV and a Gaussian, multiplied by a total and partial covering absorbers ($\chi^2_\nu = 1.15$ for 995 d.o.f.). No further component is required by the fit. The spectral parameters are reported in Table 3. The blackbody component, significant at 8σ confidence level, has a radius of 40^{+20}_{-10} km (at 1 kpc).[4] The Gaussian accounts for the prominent emission feature at 6.4 keV with no significant energy shift. The total absorber column density is consistent with the galactic value in the direction of the source derived from Kalberla et al. (2005) and Dickey & Lockman (1990). No significant change with time is found in the spectral parameters within their statistical uncertainties.

The spectral analysis reveals that the X-ray emitting region is small and the plasma reaches typical temperatures achieved in a magnetically confined accretion flow, where a standing shock is formed at the poles of the compact star. Since the derived temperature of the hot component has to be regarded as a lower limit to the maximum temperature of the post-shock region, we also used the model of Suleimanov, Revnivtsev & Ritter (2005) (private code to be used into xspec). This model takes into account the growth of pressure towards the WD surface and hence the change of gravity, allowing us to obtain a more reliable value for the maximum temperature and consequently an estimate of the WD mass. Since the model is computed for the continuum only, we then added a broad Gaussian to take into account the iron complex (thermal and fluorescence). A fit to the *XMM–Newton* EPIC and *Swift* BAT spectrum for $E > 3$ keV gives a mass $M = 0.64^{+0.03}_{-0.04}\,{\rm M}_\odot$ ($\chi^2_\nu = 1.48$, 636 d.o.f.).

We inspected spectral parameters variability by comparing the *XMM–Newton* EPIC and *Swift* XRT spectra. Due to the low source count rate, we accumulated an average XRT spectrum over all the *Swift* pointings in 2008, excluding the 2012 ones where the

[4] A distance of $1.15^{+0.67}_{-0.42}$ kpc has been estimated by Thorstensen et al. (2010).

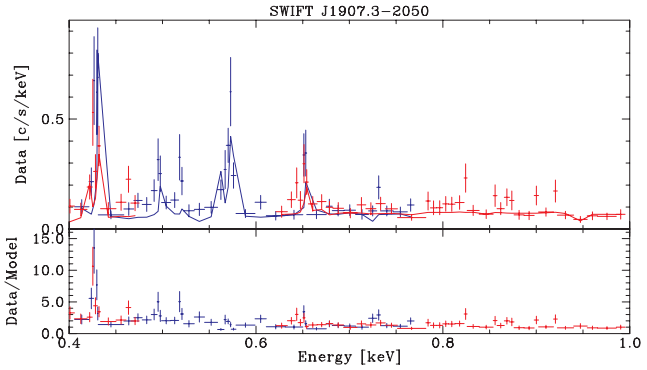

Figure 6. *XMM–Newton*/RGS spectra of Swift J1907 in the 0.4–1.0 keV region. RGS1 data are shown in blue, RGS2 in red. The top panel shows data with a model in which nitrogen abundance was left as free parameter, with a best-fitting value of ∼2, while the abundances of other elements remain fixed at 0.7. The bottom panel shows the data to model ratio when the abundance of all elements were set to 0.7.

count rate is much lower. We used the same model used for the EPIC spectrum, but did not include the 6.4 keV iron line and the BB component because they are not statistically required. We left free to vary all parameters except for the abundances that were fixed at the *XMM–Newton* best-fitting values. The spectral fit has a $\chi^2_\nu = 1.08$ for 114 d.o.f. The temperature of the hot MEKAL is consistent, within uncertainties, with that found from the *XMM–Newton* spectral fit, ($kT_{\rm h} = 14^{+4}_{-2}$ keV), while the temperature of the cold MEKAL is unconstrained, likely due to the low S/N. A 3σ upper limit is $kT_{\rm c} < 0.11$ keV. The 0.3–10 keV *Swift* flux ($\sim 7.9 \pm 0.3 \times 10^{-12}$ erg cm^{-2} s^{-1}) is a factor of ∼3 fainter than that of *XMM–Newton* (see Table 3). We also extracted the 2012 June XRT spectrum but used a simple power law, due to the extremely low S/N. At this epoch, the flux is $6.1^{+7.9}_{-3.3} \times 10^{-14}$ erg cm^{-2} s^{-1}, indicating a decrease by a factor of ∼100, in a three-months time-scale. The *Suzaku* spectrum when fitted with the same components of *XMM–Newton* spectrum gives an average 0.3–10 keV flux of 2.3×10^{-11} erg cm^{-2} s^{-1}, consistent with that obtained from the *XMM–Newton* data. From the long-term X-ray history (see also Fig. 4), we then conclude that Swift J1907 is also a highly variable X-ray source on months–years time-scale.

3.1.4 The RGS spectrum of Swift J1907

We have applied the best-fitting EPIC model (Table 3) to the RGS spectra of Swift J1907 (Fig. 6). Although the overall trend is reproduced by the model, there are significant residuals and χ^2_ν remains relatively high (∼1.3). The most prominent residuals correspond to the He-like lines of nitrogen (E ∼ 0.425 keV). Using the variable abundance version of MEKAL model, fixing the abundances at 0.7 except that of nitrogen, we find a significant overabundance of this element (∼2 times Solar). While the χ^2_ν is still not satisfactory (∼1.2), the modest quality of the RGS spectra and the large number of free parameters do not allow further possible refinement.

3.2 Swift J1212.3−5802

3.2.1 X-ray, UV and Optical timing analysis

The combined EPIC PN and MOS light curve in the 0.3–15 keV range (Fig. 7) shows the presence of a long-term variability on which rapid changes by a factor of 2, occur on a time-scale of tens

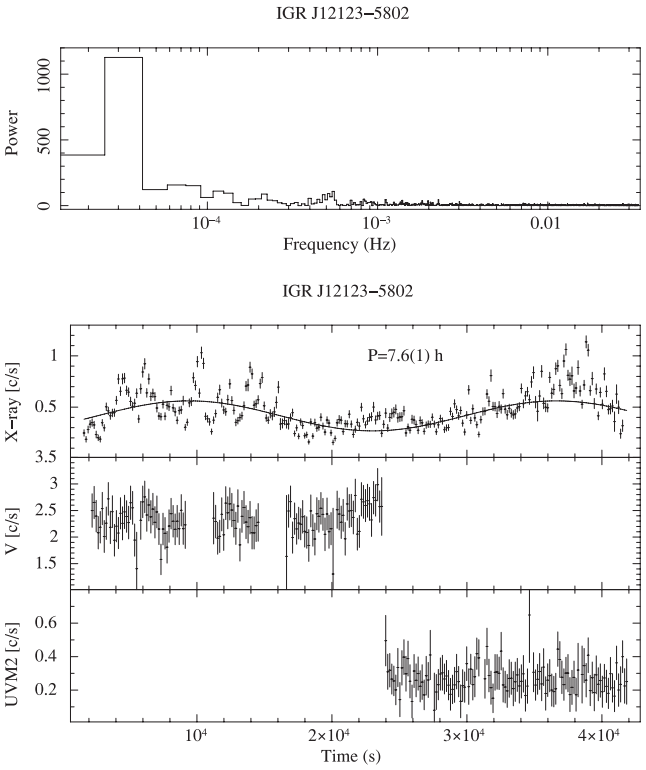

Figure 7. Upper Panels: IGR J1212 PN 0.3–15 keV power spectrum. Lower Panels: IGR J1212 PN plus MOS 0.3–15 keV background-subtracted light curve (top), *V* band light curve (centre) and *UVM2* light curve (bottom). The binning time is 150 s in all bands. The solid line represents a fit made by a constant plus a sinusoid function (solid line).

of minutes. In the first 13 ks of observation, the average count rate is ∼1.0 cts s^{-1}, between 13 and 30 ks the count rate is ∼0.6 cts s^{-1}, while between 30 and 41 ks it is again ∼1.0 cts s^{-1}. The power spectrum shows a peak at $\sim 3.5 \times 10^{-5}$ Hz, ∼8 h (see Fig. 7 and Table 2). A sinusoidal fit to the 0.3–15 keV light curve gives a period of 7.6 ± 0.1 h, 3σ cl. Given that the *XMM–Newton* observation is 11.1 h long, we cannot assess if this variability is truly periodic.

The power spectrum of the light curve detrended from the main variability (7.6 h) does not reveal significant peak. A short-term variability seems to be present during the high rate sections of the observation ($t \lesssim 18$ ks, $t \gtrsim 30$ ks) and the corresponding power spectrum peaks at 1900 s. However, this peak is only present in the first section. Hence, it is likely that at high rates IGR J1212 is affected by QPO-like variability. We also inspected the behaviour of HR with time, using both 1–3 keV/0.3–1 keV and 5–15 keV/3–5 keV ratios. No change is found within statistical uncertainties.

The OM *V*- and *UVM2*-band photometry has low statistics, due to the faintness of the source ($V = 17.1$ mag and $UVM2 = 17.2$ mag), and does not show the changes observed in the X-rays (Fig. 7). We also analysed ground-based *B* band differential photometry acquired on 2011 May 24–26 at the 2.15 m telescope at the Complejo Astronomico el Leoncito, *CASLEO*, in Argentina, equipped with a direct CCD camera. IGR J1212 was observed for about 5 h each night. Exposure times of individual images were 60, 90 and 120 s, respectively. The *B*-band light curve (not shown) displays flickering-type variability on time-scales from few minutes to tens of minutes with no clear periodic trend during the three nights.

Table 4. IGR J1212: spectral parameters of the best-fitting models. Uncertainties are 1 sigma confidence level.

IGR J1212					
CEMEKL			2 MEKAL		
N_{H_w}	10^{22} cm^{-2}	0.11 ± 0.01	N_{H_w}	10^{22} cm^{-2}	0.11 ± 0.01
$N_{H_{Pc}}$	10^{22} cm^{-2}	2.3 ± 0.4	$N_{H_{Pc}}$	10^{22} cm^{-2}	2.8 ± 0.5
cvf	per cent	53 ± 3	cvf	per cent	49 ± 2
			kT_c	keV	5.95 ± 0.02
kT_{max}	keV	>43	kT_h	keV	>62
norm	10^{-3}	6.4 ± 0.3	$norm_c$	10^{-3}	0.5 ± 0.2
			$norm_h$	10^{-3}	2.6 ± 0.5
A_Z		1.0 ± 0.3	A_Z		1.5 ± 0.4
EW[a]	keV	0.25 ± 0.03	EW	keV	0.21 ± 0.03
$F_{0.3-10}$	10^{-11}	0.46 ± 0.01	$F_{0.3-10}$	10^{-11}	0.46 ± 0.02
			F_{15-100}	10^{-11}	0.77 ± 0.01
F_{bol} [b]	10^{-11}	1.5 ± 0.1	F_{bol}^{c+h} [c]	10^{-11}	1.6 ± 0.1
χ^2_ν (d.o.f.)		0.93 (261)	χ^2_ν (d.o.f.)		0.87 (259)

[a]Energy of the Gaussian fixed at 6.4 keV.
[b]Unabsorbed bolometric flux of CEMEKL model.
[c]Unabsorbed bolometric flux of the MEKAL components.

3.2.2 *X-ray spectral analysis*

We found two spectral models that are equally statistically acceptable. The first one is composed by a multitemperature optically thin plasma in which the emission measure follows a power law in temperature (CEMEKL) plus a Gaussian at 6.4 keV to account for the fluorescent 6.4 keV Fe line. The power-law index α, when left free to vary is consistent within errors to unity. We, therefore, fixed it at this value. The second one is made by the sum of two MEKAL and a Gaussian at 6.4 keV. Both models required a complex absorption made of a total (WABS) and a partial covering (PCFABS) absorbers. In both cases, the inclusion of a blackbody component is not statistically required, its significance being $<2\sigma$. Spectral fit results are reported in Table 4 and shown in Fig. 5 (CEMEKL model only).

The hydrogen column density of the total absorber is lower than the total galactic column density in the direction of the source (3.2–4.1 10^{22} cm^{-2}), suggesting an interstellar origin. On the other hand, the N_H of the partial covering absorber (cvf $= 49-53$ per cent) indicates it is local. For both models, CEMEKL and two-MEKAL, the high-temperature component is unconstrained. Lower limits of 43 and 62 keV are found, respectively. The 6.4 keV fluorescent Fe line is strong in this source (EW = 250 eV) indicating that reflection is not negligible. However, a reflection component is not statistically significant in the fits. In both cases, the abundances are, within uncertainties, consistent with the solar value. We are unable to prefer one of the two models with current data. To estimate the WD mass, we applied also for this source the Suleimanov et al. (2005) model obtaining $M_{WD} = 0.89^{+0.02}_{-0.04}$ M$_\odot$. The 0.2–10 keV spectrum, extracted between 0–14 ks (high rate) and 14–30 ks (low rate), if fitted with the same model does not reveal spectral changes within statistical uncertainties, except for the normalization. Hence, the large variability observed during the *XMM–Newton* exposure is due to changes of the emitting volume.

3.3 IGR J19552+0044

3.3.1 *X-ray timing analysis*

IGR J1955 is also a highly variable source. The 0.3–15 keV combined EPIC PN and MOS light curve displays a large amplitude variation over the whole observation where count rate increases by a factor of ∼3 (Fig. 8). A dip lasting ∼1.5 ks is also observed at ∼10 ks since the start of the observation. The count rate decreases by ∼9.7 times the average value, almost reaching zero counts. A short-term (few hours) variability is also present.

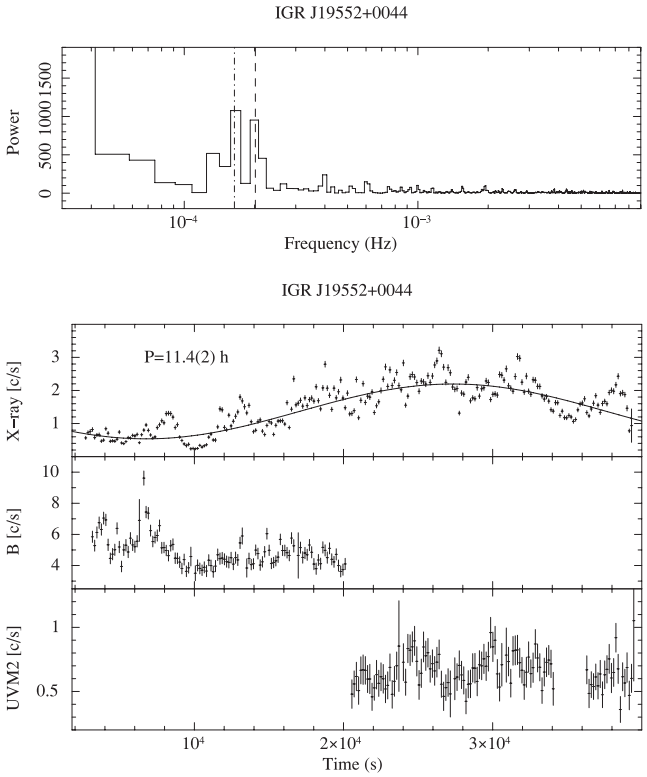

Figure 8. Upper Panel: IGR J1955 PN 0.3–15 keV power spectrum. The dashed and dot dashed lines at $\sim 1.7 \times 10^{-4}$ Hz and 2×10^{-4} represent the 1.69 and 1.32 h periods, respectively. Lower Panels: IGR J1955 PN plus MOS 0.3–15 keV background-subtracted light curve (top), *B*-band light curve (centre) and *UVM2* light curve (bottom). The binning time is 150 s in all bands. The solid line represents a fit made by a constant plus a sinusoid function (solid line).

The X-ray power spectrum shows three main peaks: a short frequency one at $\sim 2.5 \times 10^{-5}$ Hz (∼11 h), and two close ones at $\sim 1.7 \times 10^{-4}$ Hz and 2×10^{-4} Hz (∼6000 s and ∼5000 s), respectively (see Fig. 8). A sinusoidal fit to the light curve gives a period of 11.4 ± 0.2 h (3σ cl). This value should be considered as an indication of a long-term variability, because of the limited *XMM–Newton* exposure. For the two short-term variabilities, both significant at 8σ cl, we obtain: 6100 ± 120 (1.69 ± 0.04 h) and 4960 ± 80 s (1.32 ± 0.08 h), see Table 2. On the other hand, the UV and *B*-band light curves are too short to allow a timing study. However, we can identify an optical counterpart (*B* band), although much shallower, to the dip observed in the X-rays (see Fig. 8).

We studied the energy dependence of the pulse shape, by fitting the light curves in the ranges 0.3–1, 1–3, 3–5 and 5–15 keV at the two periods. The pulse at 4960 s is phase aligned and structured at all energies, with a double-peaked maximum at phases ∼0.0 and ∼0.3, respectively. The pulse fraction PF slightly decreases with energy: $PF_{0.3-1} = 18.2 \pm 0.8$ per cent, $PF_{1-3} = 16.5 \pm 0.8$ per cent, $PF_{3-5} = 20 \pm 2$ per cent, $PF_{5-15} = 13 \pm 2$ per cent. The average PF in the 0.3–15 keV range is 17.0 ± 0.5 per cent. The HR between

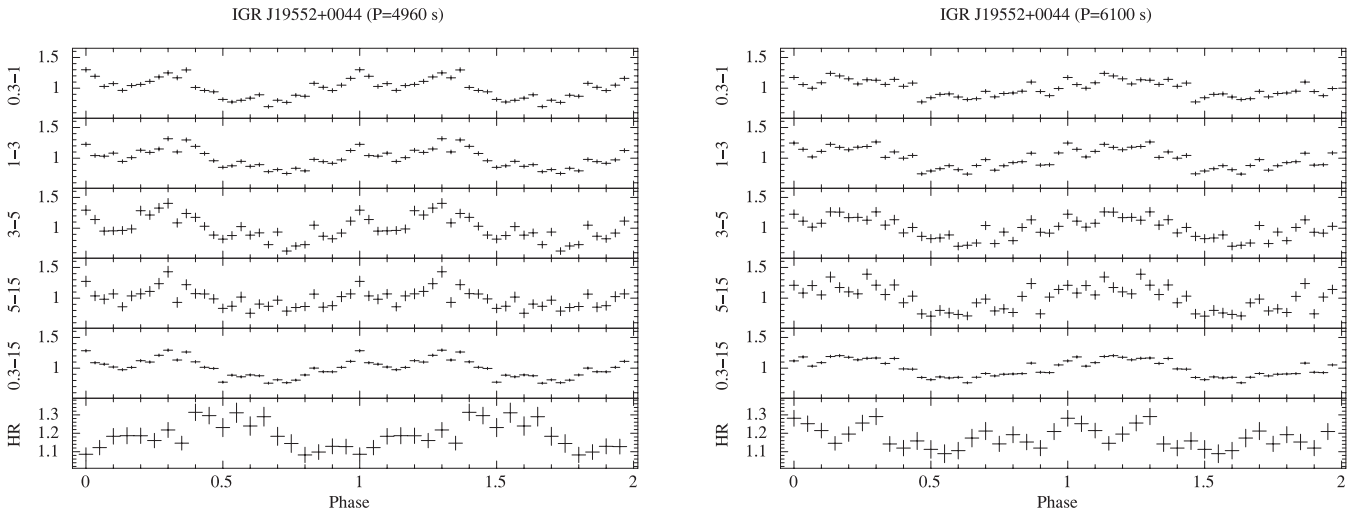

Figure 9. Left panels: from top to bottom, IGR J1955 pulse profiles folded at 4960 s in five energy intervals, 0.3–1, 1–3, 3–5, 5–15, 0.3–15 keV, on the *y*-axis the normalized intensities. On the bottom line the hardness ratio (HR) for the 1–3 keV versus 0.3–1 keV band. Right panels: The same as left panels, but for the 6100 s period.

1–3 and 0.3–1 keV indicates a tendency of spectral hardening (significant at 3.6σ level) close to pulse minimum, $\phi = 0.4$–0.6 (see Fig. 9). The low S/N does not allow us to infer changes in the HR between 5–15 and 3–5 keV bands.

The pulse at 6100 s is instead less structured and roughly single peaked, with the maximum at $\phi = 0.2$, phase aligned at all energies. The PF slightly increases with energy: $PF_{0.3-1} = 14.6 \pm 0.8$ per cent, $PF_{1-3} = 18.5 \pm 0.8$ per cent, $PF_{3-5} = 20 \pm 2$ per cent, $PF_{5-15} = 22 \pm 2$ per cent. The average PF in the total 0.3–15 keV band is 17.1 ± 0.5 per cent. A marginally significant (2.4σ) spectral hardening at pulse maximum is found from the HR between 1–3 and 0.3–1 keV bands.

Finally, the HR between 1–3 and 0.3–1 keV over the whole *XMM–Newton* observation reveals a hardening when flux increases. The ratio between the two light curves is 0.78 ± 0.03 during the first 6 ks, while later it is 1.18 ± 0.02.

3.3.2 X-ray spectral analysis

The best-fitting model is made of a multitemperature (CEMEKL) plasma absorbed by a total absorber (WABS) and a Gaussian to account for the excess at 6.4 keV. The inclusion of a partial covering absorber (PCFABS) is not statistically required. The power-law α index is 0.74 ± 0.05 and its inclusion as free parameter is significant at 4.8σ. The $N_{\rm H}$ column density is $0.07 \pm 0.02 \times 10^{22}$ cm^{-2}, and is lower than the total galactic column density in the direction of the source ($0.13-0.16 \times 10^{22}$ cm^{-2}). The fluorescent 6.4 keV Fe line is moderately weak (EW $= 70 \pm 20$ eV). A soft blackbody component is not required. All model parameters are reported in Table 5 (see also Fig. 5). Similarly to the other sources, we also applied the Suleimanov et al. (2005) model to derive the WD mass, and find $M_{\rm WD} = 0.77^{+0.02}_{-0.03}\,{\rm M}_{\odot}$ ($\chi^2_\nu = 1.09$, 489 d.o.f.).

We also investigated phase-dependent spectral variability at the 4960 s period, by selecting the phase intervals $\phi = 0.0-0.5$ and $\phi = 0.5-0.9$ corresponding to the maximum and minimum, respectively. We fixed at their average values the hydrogen column density $N_{\rm H}$, the metal abundance $A_{\rm Z}$, and the Gaussian energy, all other parameters were left free to vary. Only the normalization was found to change (∼20 per cent) according to the flux variation.

Table 5. IGR J1955: spectral parameters of the best-fitting model. Uncertainties are 1 sigma confidence level.

	IGR J1955 CEMEKL	
$N_{\rm H}$	10^{22}cm^{-2}	0.076 ± 0.003
$kT_{\rm max}$	keV	36 ± 4
norm	10^{-3}	9.9 ± 0.4
α		0.74 ± 0.05
$A_{\rm Z}$		0.62 ± 0.07
EW[a]	keV	0.07 ± 0.02
$F_{0.3-10}$	10^{-11}	1.06 ± 0.01
$F_{\rm bol}$ [b]	10^{-11}	2.2 ± 0.1
χ^2_ν (d.o.f.)		1.05 (725)

[a]Energy of the Gaussian fixed at 6.4 keV.
[b]Unabsorbed bolometric flux of CEMEKL model.

The RGS spectra have low S/N but broadly confirm the EPIC spectral fits. The strongest lines seen are those of O VII, O VIII and Fe XVII (0.83 keV = 15A). Some lines (N VII, O VII, Mg XI and Mg XII) may be stronger than that in the best-fitting model. However, this should be re-examined with higher S/N data.

4 DISCUSSION

4.1 Swift J1907.3−2050: a long period magnetic CV?

The X-ray history of Swift J1907 over ∼5 yr reveals a highly variable X-ray source on both short (hours) and long (months–years) time-scales. We detect a transient feature with characteristic time-scale of ∼2 h in the *XMM–Newton* X-ray and optical data. It may also be present in the *Suzaku* and *Swift* XRT data at some epochs. The possibility that it represents the spin period of the WD is highly unlikely, since the spin signal is not expected to disappear without a significant change in the source state. The characteristic 2 h time-scale is close to the free-fall time from the inner Lagrangian point. Indeed, with a WD mass of 0.64 $M_{\odot}$ and a donor star mass

of 0.8 $M_\odot$ (Thorstensen et al. 2010), this binary would have an inverted mass ratio $q = M_{sec}/M_{WD} = 1.3$. The WD Roche Lobe radius would be 1.8×10^{11} cm and the free-fall time ∼5900 s. The occurrence of this feature at high rates (both in the X-rays and UV/optical) suggests a transient enhancement of mass transfer from the donor star overflowing the accretion disc. For the latter, we estimate a colour temperature of 12 kK from the lowest observed UV and *B*-band fluxes corrected for reddening.[5] The flare activity also indicates that mass accretion rate changes are not uncommon on time-scales of hours.

Swift J1907 also varies on a longer time-scale ($\gtrsim$8 h) in both X-ray and optical/UV ranges and we could detect a flare-like activity lasting ∼6 h in the *Suzaku* data. With the present data, we cannot assess whether it is related to the long 20.82 h orbital period. Due to the lack of energy dependence, the flare is likely due to a temporary enhancement in the accretion rate, rather than resulting from an orbital modulation.

Swift J1907 was already known to display high, intermediate and low optical states, where accretion partially or completely switches-off in some occasions (see Thorstensen et al. 2010, and reference therein). The X-ray history also shows that it undergoes high and low X-ray states on a months–years time-scale, thus corroborating mass accretion rate changes. This peculiarity is typical of magnetic systems of the Polar-type or nova-like CVs of the VY Scl-type stars (see e.g. Honeycutt & Kafka 2004). The orbital period of 20.82 h is by far longer than those of VY Scl stars, which cluster at the 3 h edge of the orbital period gap, and also longer than those of Polars, being V1309 Ori (8 h) the longest period Polar known so far.

The spectral characteristics of Swift J1907 may favour a magnetic system as early suggested by Thorstensen et al. (2010). A high complex absorbing material, is a defining characteristic of magnetic systems, particularly of IPs, rather than of non-magnetic CVs (see Ramsay et al. 2008). Also a multitemperature plasma reaching high temperatures (∼14 keV) is typical of accretion shocks at the WD poles. An optically thick component, with temperature of 60 eV and with a small emitting area, is also a characteristic of magnetic systems only. This component is a recognized feature in Polars and recently in IPs. However, an orbitally locked WD rotation at the extremely long 20.82 h period would imply a very high magnetic field, $\gtrsim 1.4 \times 10^{10}$ G (see Warner 1995). No WD in CVs has ever been detected with such magnetic field strength, being the highest field Polar AR UMa with $B = 2.3 \times 10^8$ G. At high field strengths, accretion shocks are cyclotron dominated and even buried at low local accretion rates (Woelk & Beuermann 1996; Fischer & Beuermann 2001). This would yield a strong soft component. We instead infer a bolometric flux ratio between the blackbody and optically thin components $F_{BB}/F_{thin} \sim 0.24$.

The remaining possibility is that Swift J1907 is an IP. This would be consistent with the spectral characteristics of this sub-type of magnetic systems. Known IPs at the longest ($\gtrsim$10 h) periods, such as GK Per (47.9 h), RX J1730−0559 (15.4 h) and AE Aqr (9.9 h), possess rapidly spinning WDs with high degree of asynchronism ($\leq$0.002), with the only exception of V1062 Tau (10 h and ∼0.1). However, no rapid X-ray pulses are detected in the X-ray power spectrum of Swift J1907.

The presence of a blackbody component at 60 eV, with a ratio between the bolometric soft and hard X-ray fluxes of about 0.24, is a key signature of magnetic accretion. Typical range of temperatures in Polars is 20–40 eV, with a few systems at ∼60 eV. In IPs, the soft component is instead found to span a wider range of temperatures up to ∼90 eV (Anzolin et al. 2008, 2009; Bernardini et al. 2012). Hence, Swift J1907 is located in the soft-to-hard X-ray luminosity ratio versus temperature plane (see Anzolin et al. 2008) mid-way between the Polars and IPs. In Swift J1907 this component arises from a small region of 40 km (a 3σ upper limit is 114 km at 1 kpc). For a WD mass of 0.64 $M_\odot$, the corresponding radius is 8.3×10^8 cm (Nauenberg 1972), implying that the reprocessed optically thick emission comes from a fractional area $f \sim 6 \times 10^{-6}$ (3σ upper limit is $f \lesssim 2 \times 10^{-4}$). It was recently demonstrated that this soft X-ray component is constituted by a range of temperatures over the accretion spot area (Beuermann, El Kholy & Reinsch 2008; Beuermann, Burwitz & Reinsch 2012). The projected fractional WD surface area in the prototypical Polar AM her is about 0.07 per cent with the hottest regions (>40 eV) arising from much smaller fractional areas, $<2 \times 10^{-6}$ (see Beuermann et al. 2012, for detail). For Swift J1907 we can only infer the average temperature of this component and a rather small and weakly constrained emitting area. These values are closer to those derived in the soft IPs (Anzolin et al. 2008), which seem to possess smaller and hotter spots than Polars. Hence, though sharing similar properties of soft emitting magnetic CVs, it cannot be unambiguously ascribed to either the IP or the Polar groups.

To help in understanding this CV, we also estimated its mass accretion rate. We assume that the accretion luminosity is represented by the X-ray bolometric luminosity, $L_{acc} = G\,\dot{M}\,M_{WD}\,R_{WD}^{-1} \sim L_{BB} + L_{thin}$, that includes both reprocessed X-ray component and that of the hard X-rays. Using the derived WD mass and radius values of 0.64 $M_\odot$ and 8.3×10^8 cm, we estimate $\dot{M} = 2 - 4 \times 10^{-9}\,M_\odot\,yr^{-1}$, for a minimum distance of 730 pc and a maximum of 1.15 kpc, respectively. This value is higher than the mass transfer rate ($\dot{M}_{sec} \sim 5 \times 10^{-10}\,M_\odot\,yr^{-1}$) expected for a donor filling its Roche lobe (Warner 1995) at an 18–20 h orbital period. It is however lower by two orders of magnitude than that predicted by magnetic braking (McDermott & Taam 1989) at the same orbital periods. Consequently, it may be possible that Swift J1907 has recently entered into a CV phase. The high nitrogen abundance is also a peculiar feature of Swift J1907. A number of CVs were found from far-UV spectra to display anomalous CNO abundance and believed to be the descendant of massive progenitor donors (Gänsicke et al. 2003). This, together with the large binary mass ratio and the long orbital period, might suggest that Swift J1907 is also descending from a progenitor binary which underwent a phase of thermal time-scale mass transfer (TTMT Podsiadlowski, Han & Rappaport 2003; Schenker, Wynn & Speith 2004).

Furthermore, long observations in the X-rays and in the optical, including polarimetry as well as UV spectroscopy, will help to understand the true nature and evolutionary status of this CV.

4.2 IGR J12123−5802 a true IP or a magnetic impostor?

IGR J1212 is a faint, but highly variable X-ray source. We find a $\gtrsim$7.6 h variability although we cannot assess whether it is related to the binary orbit. Variations on time-scales of ∼1900 s are not periodic. None of these variabilities have an optical counterpart where only flickering on time-scale of a few minutes is found.

On the other hand, the broad-band X-ray spectrum is hard and well described by a multitemperature plasma with a high, although unconstrained, maximum temperature. We also infer a high mass for

[5] We adopt an extinction of $E(B-V) = 0.14$, as derived from the hydrogen column density from X-ray spectral fits (Ryter, Cesarsky & Audouze 1975).

the WD (0.89 $M_\odot$). The spectrum is highly absorbed by interstellar and local material, the latter covering ∼50 per cent the X-ray source. A strong (EW = 250 eV) Fe fluorescent line is also present suggesting that reflection from cool material is present in this system. A high column density partial absorber and an intense Fe fluorescent line are defining characteristics of magnetic CVs (Ezuka & Ishida 1999). Hence, a magnetic system might be favoured. The lack of detection of a blackbody component also does not favour a Polar-type CV. While the lack of detection of a coherent periodicity does not allow us to classify IGR J1212 as an IP, we here note that other systems, such as LS Peg, EI UMa and V426 Oph (Ramsay et al. 2008), have also failed to show coherent periodicities and due to the spectral characteristics similar to IPs, were defined as 'bona fide' IPs. For V426 Oph and LS Peg, it is also speculated that the lack of pulsations could be due to the close alignment of the magnetic and rotation axes.

The high temperature derived from X-rays if due to magnetic accretion would imply a mass of 0.89 $M_\odot$, that would locate IGR J1212 within the range of most CV primary masses (Zorotovic, Schreiber & Gänsicke 2011). On the other hand, if this temperature is achieved through a Keplerian disc accretion it would give a WD mass of ∼1.2 $M_\odot$. Few CVs are known to harbour such massive WDs (Zorotovic et al. 2011).

Optical spectroscopy and polarimetry, as well as long photometric runs, could help to shed light into this new CV.

4.3 IGR J19552+0044: a long period IP or a magnetic CV below the gap?

We have detected periodic variabilities at 1.69 h (6100 s), 1.38 h (4960 s). A large amplitude variability on time-scale of 11 h is also present. Support to both the short- and the long-term variabilities also comes from optical ground-based photometry and spectroscopy (Tovmasian et al. in preparation, private communication). The X-rays arise from a multitemperature plasma with maximum temperature of 36 keV suffering little absorption of interstellar origin. The 1.38 h periodicity is due to changes in the normalization of the emitting plasma. These features are rather similar to HT Cam (de Martino et al. 2005), a low accretion rate IP below the orbital period gap. The bolometric X-ray luminosity is $4.3 \times 10^{31}\, d^2_{100\,\mathrm{pc}}$ erg s^{-1}. If it represents the accretion luminosity, for $M_{\mathrm{WD}} = 0.8\,M_\odot$ and $R_{\mathrm{WD}} = 7 \times 10^8$ cm (Nauenberg 1972), the accretion rate would indeed be very low: $4.5 \times 10^{-12}\, d^2_{100\,\mathrm{pc}}\, M_\odot$ yr^{-1}.

The X-ray periodicities of 1.69 h, 1.38 h and the ∼11 h variability are, however, difficult to interpret. We here propose and discuss two possibilities.

4.3.1 A long-period IP or a pre-Polar?

If 1.38 h represents the spin of the accreting WD and 1.69 h is a sideband period ($P_{\omega-\Omega}$ or $P_{\omega-2\Omega}$), the orbital period would be either 7.3 h or 14.6 h. The detected variability at 11 h or longer, if periodic, would suggest the second case. However, such long-period system is expected to have a high accretion rate and a main-sequence G3-5-type donor star (Smith & Dhillon 1998). A re-analysis of the optical spectra by Masetti et al. (2010) does not reveal G-type star features but only weak absorptions in the red portion, possibly suggesting Ca I 6162 and TiO 6900 Å. Hence a G-type star is rather unlikely. The Two Micron All Sky Survey (2MASS) measures give only an upper limit to the *J*-band magnitude ($J < 17.03$), implying a lower limit to the distance of 6.4 kpc which seems to be in contradiction with the inferred low absorption. Furthermore, the ratios of He II and H_β line fluxes and equivalent widths (EWs) are closer to those found in Polars rather than in IPs (van Paradijs & Verbunt 1984) and the overall spectrum very much resembles those of Polars. Also, IGR J1955 is found at $B = 17.6$ mag, at similar flux level when observed by Masetti et al. (2010) in 2009, but much fainter than in the USNO (15.6 mag) and in the Sloan Digital Sky Survey (SDSS) catalogues ($g = 15.9$ mag). A 1.6–2 mag difference suggests a highly variable source, that is more common to short period CVs.

Alternative possibility is that the 1.38 h and the 1.69 h periods are the spin and the orbital periods, respectively. A short period magnetic CV could reconcile the low accretion rate and the absence of intrinsic absorption derived from X-rays. The beat period would then be 7.29 h, not detected but the long-term variability could be a sign of a sub-harmonic, although difficult to interpret. Clearly a longer observation would solve the true nature of the long-term variability. If it were the case the spin-to-orbital period ratio would be 0.82. The period of 1.69 h would locate this source below the orbital period gap, where most Polars are found and only five IPs. The latter have spin-to-orbit period ratio ranging from 0.1 (HT Cam) to 0.68 (EX hya). On the other hand, only five Polars are known to possess desynchronized primaries (CD Ind, BY Cam, V1500 Cyg, V4633 Sgr and V1432 Aql) with spin-to-orbital period ratios between 0.98 and 1.02. IGR J1955 would then be either an extremely low asynchronous IP or the most asynchronous Polar. Only one system is known to share a similar property, Paloma also known as RX J0524+42 (Schwarz et al. 2007). Its spin-to-orbit period ratio of 0.93–0.97 (depending on the true spin period) and its orbital period of 2.6 h locate it in the period gap. Paloma is believed to be a transition object between IPs and Polars. As no IP is theoretically expected below the orbital period gap, the few IPs will likely never synchronize (Norton, Wynn & Somerscales 2004; Norton et al. 2008). However, IGR J1955 being so close to the line of synchronization could still evolve towards synchronism. In this case, magnetic field measurements through polarimetry are crucial.

The X-ray analysis also reveals a hard X-ray spectrum but no soft X-ray blackbody component. Three of the asynchronous Polars mentioned above (CD Ind, BY Cam, and V1432 Aql) display unusually hard X-ray spectra and are detected above 20 keV in the *INTEGRAL*/IBIS or Swift/BAT surveys. Interestingly also Paloma has been detected by *Swift*/BAT and has been recently catalogued in the latest 70-month BAT catalogue (Baumgartner et al. 2013).

4.3.2 A magnetic evidence from IR

IGR J1955 is reported in the 2MASS catalogue with $J < 17.03$ mag, $H = 15.63 \pm 0.11$ mag and $K = 14.07 \pm 0.06$ mag. The *J* band upper limit could be due to the drop of the UV–optical spectrum at these wavelengths, but the 2MASS colour index $(H - K) = 1.56$ does not support the contribution from any donor late-type star (see Straižys & Lazauskaitė 2009). If the 2MASS *J* band upper limit is attributed to an M5 star (for an orbital period of 1.69 h), the minimum distance is then 400 pc. This is more compatible with the low interstellar absorption derived from the X-rays.

The peculiar shape of the nIR spectrum is further confirmed by the surprising detection of IGR J1955 at IR wavelengths by the *Wide-field Infrared Survey Explorer* (*WISE;*Wright et al. 2010) in all the four bands, *W*1 (3.35 μm), *W*2 (4.6 μm), *W*3 (11.6 μm) and *W*4 (22.1 μm) and catalogued as WISE J195512.47+004536.6. The corresponding magnitudes are $m_{\mathrm{W1}} = 11.556 \pm 0.024$, $m_{\mathrm{W2}} = 11.031 \pm 0.023$, $m_{\mathrm{W3}} = 9.704 \pm 0.041$ and $m_{\mathrm{W4}} = 8.506 \pm 0.31$. Most WDs detected by *WISE* (the *WISE*

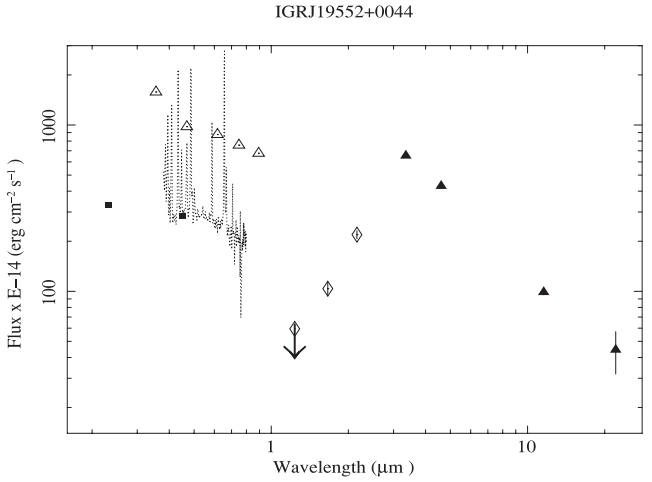

Figure 10. The SED of IGR J1955 constructed with the *XMM–Newton* UV and *B*-band fluxes (filled squares), the optical spectrum by Masetti et al. (2010) (dotted line), the SDSS photometry (empty triangles), the 2MASS nIR (empty diamonds) and *WISE* measures (filled triangles). No correction for extinction is applied. The peculiar shape is discussed in the text.

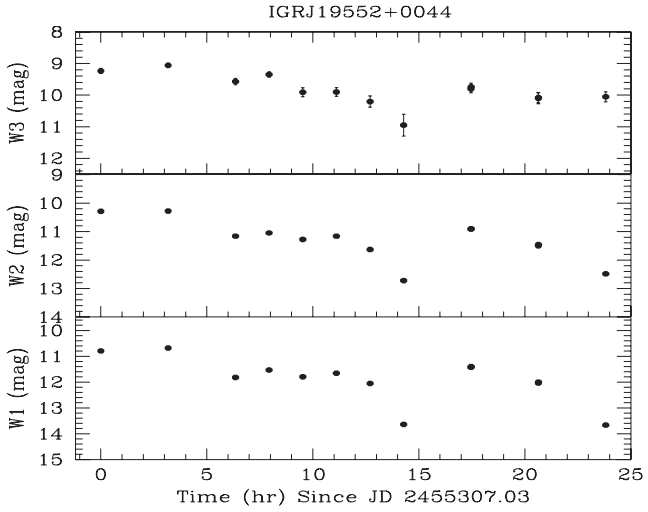

Figure 11. The *WISE* light curve of IGR J1955 constructed using the 'single exposures' in the *W*1, *W*2 and *W*3 bandpasses, showing large IR variability.

InfraRed Excesses around Degenerates, WIRED, survey project) are WD + mainsequence binaries (Debes et al. 2011). Infrared excess around WDs could also be due to debris discs (Debes et al. 2012) or cyclotron emission in case of magnetic systems (Harrison et al. 2013). Therefore, we have combined the OM UV and *B*-band photometry, the SDSS (u′,g′,r′,i and z′) and optical spectrum by Masetti et al. (2010) with the 2MASS (*J*, *H* and *K*) and WISE (*W*1,*W*2, *W*3 and *W*4) photometry to construct the spectral energy distribution (SED), although these measures are taken at different epochs.[6] (see Fig. 10). The SED is not corrected for extinction because, from the hydrogen column density of X-ray fits, it is at most $E(B-V) = 0.1$. Nevertheless, the unusual shape of the SED is apparent, with a pivot energy at 1.2 μm, where at shorter wavelengths the spectrum is a power-law $F_\nu \propto \nu^\alpha$, with $\alpha = 0.9$ for the OM UV and *B*-band data, and $\alpha = 1.5$ for the SDSS data. The rapid rise of the flux beyond 1.2 μm and the peak in the *W*1 (3.35 μm) is very similar to that observed in the Polar EF Eri with *WISE* and *Spitzer* (Harrison et al. 2013). EF Eri is a short-period (1.35 h) Polar believed to harbour a sub-stellar secondary star and which has been in a prolonged low state for a decade. The nIR and IR spectrum of EF ERi also does not give evidence of the secondary star but has been modelled as due to cyclotron emission from accretion on to a 12.6 MG WD (see Harrison et al. 2013, for more details). At these wavelengths, the contribution comes from lower cyclotron harmonics ($n = 1, 2, 3$), which are expected to be optically thick. The lack of nIR and IR spectroscopy does not allow a meaningful analysis of the spectrum of IGR J1955 with cyclotron models. Also, since EF Eri is strongly variable (more than a magnitude) in the nIR and IR along its orbital period, we have then inspected the 'single exposure' observations from *WISE* survey. These were acquired along 1 d on 2010 April 21. Useful data are reported for the *W*1, *W*2 and *W*3 bandpasses in Fig. 11, that show large variations ($\Delta M > 1$ mag). Unfortunately, the data are too sparse to phase them at either 1.38 h or 1.69 h periods.

[6] The SDSS data were taken in 2004 September, the 2MASS data in 1999 August, the WISE photometry in 2010 April and the optical spectroscopy in 2009.

Hence, the two short periodicities, the X-ray spectral characteristics and the striking similarity of the nIR and IR properties of IGR J1955 with EF Eri favours a magnetized CV accreting at a low accretion rate below the orbital period gap.

5 SUMMARY

We have presented the first long X-ray observations of the three new hard X-ray sources Swift J1907, IGR J1212 and IGR J1955 together with UV, optical, nIR and IR photometry.

All three sources are hard X-ray emitting CVs that show large amplitude variabilities on time-scales of minutes to hours. Two of them, Swift J1907 and IGR J1955, also show long (months to years) variabilities. Their broad-band X-ray spectra present characteristics typical of magnetic CVs. We here summarize the main results.

(i) Swift J1907 is a long (20.82 h) orbital period CV. We detected a non-coherent variability at a period of ∼7200 s. It is likely of transient nature, reflecting matter travelling from the secondary star on to the compact object. Swift J1907 reveals a spectrum closely resembling those of magnetic CVs, including a soft X-ray component originating from a small fraction of the WD area. A magnetic system is then favoured although we cannot give a proper classification. The supra-solar abundance of nitrogen (about twice the solar value), the inverted mass ratio ($q = 1.3$) and the long orbital period could suggest that Swift J1907 underwent a TTMT phase.

(ii) IGR J1212 reveals an X-ray variability at $\gtrsim$7.6 h that might reflect the binary orbital period. No fast coherent pulses are detected though, but its spectral characteristics give support to a magnetic CV of the IP type.

(iii) IGR J1955 shows two X-ray periods: 1.38 h and 1.69 h. Its X-ray spectrum indicates a system accreting at low rate similarly to the CVs below the orbital period gap. We have found IGR J1955 to display peculiar nIR and IR spectrum remarkably similar to that observed in the Polar EF Eri. We propose this system to be a pre-polar or an IP with the lowest degree of asynchronism, resembling the peculiar magnetic CV Paloma.

Our study of newly discovered CV candidates has revealed new features, departing from canonical view of magnetic CVs. In general, most of the hard X-ray discovered CVs are being found at

relatively long orbital periods. This aspect deserves a detailed investigation to understand the evolutionary status of these CVs.

ACKNOWLEDGEMENTS

This work is based on observations obtained with *XMM–Newton* an ESA science mission with instruments and contributions directly funded by ESA Member States; with *Swift*, a NASA science mission with Italian participation; and *Suzaku*, a collaborative mission between the space agencies of Japan (JAXA) and the USA (NASA). This publication also makes use of data products from the *Wide-field Infrared Survey Explorer*, which is a joint project of the University of California, Los Angeles and the Jet Propulsion Laboratory/California Institute of Technology, funded by the National Aeronautics and Space Administration; the Two Micron All Sky Survey (2MASS), a joint project of the University of Massachusetts and the Infrared Processing and Analysis Center (IPAC)/Caltech, funded by NASA and the NSF; and the Sloan Digital Sky Survey (SDSS).

REFERENCES

Anzolin G., de Martino D., Bonnet-Bidaud J.-M., Mouchet M., Gänsicke B. T., Matt G., Mukai K., 2008, A&A, 489, 1243
Anzolin G., de Martino D., Falanga M., Mukai K., Bonnet-Bidaud J.-M., Mouchet M., Terada Y., Ishida M., 2009, A&A, 501, 1047
Barlow E. J., Knigge C., Bird A. J., J Dean A., Clark D. J., Hill A. B., Molina M., Sguera V., 2006, MNRAS, 372, 224
Barthelmy S., 2000, in Flanagan K. A., Siegmund O., eds, Proc. SPIE, Vol. 4140, X-ray and Gamma-Ray Instrumentation for Astronomy XI. SPIE, Bellingham, p. 50
Baumgartner W., Tueller J., Markwardt C., Skinner G., Barthelmy S., Mushotzky R., Evans P., Gehrels N., 2013, ApJS, 297, 19
Bernardini F., de Martino D., Falanga M., Mukai K., Matt G., Bonnet-Bidaud J.-M., Masetti N., Mouchet M., 2012, A&A, 542, A22
Beuermann K., El Kholy E., Reinsch K., 2008, A&A, 481, 771
Beuermann K., Burwitz V., Reinsch K., 2012, A&A, 543, A41
Bird A. J. et al., 2010, ApJS, 186, 1
Cusumano G. et al., 2010, A&A, 524, 64
de Martino D. et al., 2005, A&A, 437, 935
de Martino D. et al., 2008, A&A, 481, 149
de Martino D. et al., 2010, A&A, 515, A25
de Martino D. et al., 2013, A&A, 550, A89
Debes J., Hoard D., Wachter S., Leisawitz D., Cohen M., 2011, ApJS, 197, 38
Debes J., Hoard D., Farihi J. S. W., Leisawitz D., Cohen M., 2012, ApJ, 759, 37
den Herder J. W. et al., 2001, A&A, 365, L7
Dickey J. M., Lockman F. J., 1990, ARA&A, 28, 215
Evans P. A. et al., 2009, MNRAS, 397, 1177
Ezuka H., Ishida M., 1999, ApJS, 120, 277
Fischer A., Beuermann K., 2001, A&A, 373, 211
Gänsicke B. et al., 2003, ApJ, 594, 443
Gehrels N. et al., 2004, ApJ, 611, 1005
Harrison T., Hamilton R., Tappert C., Hoffman D., Campbell R., 2013, AJ, 145, 19
Honeycutt R. K., Kafka S., 2004, AJ, 128, 1279
Hong J., 2012, MNRAS, 427, 1633
Hong J., van der Berg M., Grindlay J., Servillat M., Zhao P., 2012, ApJ, 746, 165
Kalberla P. M. W., Burton W. B., Hartmann D., Arnal E. M., Bajaja E., Morras R., Pöppel W. G. L., 2005, A&A, 440, 775
Koyama K. et al., 2007, PASJ, 59, 23
Luna G. J. M., Sokoloski J. L., Mukai K., Nelson T., 2012, preprint (arXiv:e-prints)
Masetti N. et al., 2006, A&A, 459, 21
Masetti N. et al., 2008, A&A, 482, 113
Masetti N. et al., 2010, A&A, 519, A96
Masetti N. et al., 2012, A&A, 538, A123
Masetti N., Nucita A., Parisi P., 2012, A&A, 544, A114
Mason K. O. et al., 2001, A&A, 365, L36
McDermott P. N., Taam R. E., 1989, ApJ, 342, 1019
Mitsuda K. et al., 2007, PASJ, 59, 1
Morihana J., Tsujimoto M., Yoshida T., Ebisawa K., 2013, ApJ, 766, 14
Nauenberg M., 1972, ApJ, 175, 417
Nebot Gómez-Morán A. et al., 2013, A&A, 553, A12
Norton A. J., Wynn G. A., Somerscales R. V., 2004, ApJ, 614, 349
Norton A. J., Butters O., Parker T., Wynn G. A., 2008, ApJ, 672, 524
Peterson B., Wanders I., Horne K., Collier S., Alexander T., Kaspi S., Maoz D., 1998, PASP, 110, 660
Podsiadlowski P., Han Z., Rappaport S., 2003, MNRAS, 340, 1214
Pretorius M. L., Knigge C., Schwope A. D., 2013, MNRAS, 432, 570
Ramsay G., Wheatley P. J., Norton A. J., Hakala P., Baskill D., 2008, MNRAS, 387, 1157
Reis R., Wheatley P., Gänsicke B., Osborne J., 2013, MNRAS, 430, 1994
Revnivtsev M., Sazonov S., Forman W., Churazov E., Sunyaev R., 2011, MNRAS, 414, 495
Ryter C., Cesarsky C. J., Audouze J., 1975, ApJ, 198, 103
Scargle J. D., 1982, ApJ, 263, 835
Scaringi S. et al., 2011, A&A, 530, A6
Schenker K., Wynn G. A., Speith R., 2004, in Vrielmann S., Cropper M., eds, ASP Conf. Ser. Vol. 315, IAU Colloq. 190: Magnetic Cataclysmic Variables. Astron. Soc. Pac., San Francisco, p. 8
Schwarz R., Schwope A., Staude A., Rau A., Hasinger G., Urrutia T., Motch C., 2007, A&A, 473, 511
Shang Y., 2002, MNRAS, 337, 609
Smith D., Dhillon, 1998, MNRAS, 301, 767
Straižys V., Lazauskaitė R., 2009, Balt. Astron., 18, 19
Suleimanov V., Revnivtsev M., Ritter H., 2005, A&A, 435, 191
Thorstensen J. R., Peters C. S., Skinner J. N., 2010, PASP, 122, 1285
Turner M. J. L. et al., 2001, A&A, 365, L27
van Paradijs J., Verbunt F., 1984, in Woosley S. E., ed., AIP Conf. Ser. Vol. 115, High Energy Transients in Astrophysics. Am. Inst. Phys., New York, p. 49
Warner B., 1995, Cambridge Astrophysics Series, Cambridge Univ. Press, Cambridge, 28
Wickramasinghe D. T., Ferrario L., 2000, PASP, 112, 873
Woelk U., Beuermann K., 1996, A&A, 306, 232
Wright E. L. et al., 2010, AJ, 140, 1868
Zorotovic M., Schreiber M., Gänsicke B., 2011, A&A, 536, A42

This paper has been typeset from a TEX/LATEX file prepared by the author.